Eurasia Journal of Science and Technology
ISSN: 2663-1016
DOI: https://doi.org/10.61784/ejst3084

SUMMER OFFICE BUILDING BASED ON ORTHOGONAL DESIGN OF DIFFERNT MODELS NUMEROCAL STUDY ON OPTIMIZATION OF AIR SUPPLY ARATERS

ShuYuan Zhang[1,2*], HanQing Wang[1,2,3], JiaXin Wei[1,2], ZiWen Zhao[1,2]
[1]School of Civil Engineering, Nanhua University, Hengyang 421001, Hunan, China.
[2]Hunan Provincial Key Engineering Laboratory of Building Environment Control Technology, Nanhua University, Hengyang 4210001, Hunan, China.
[3]School of Civil Engineering, Central South University of Forestry Science and Technology, Changsha 410000, Hunan, China.
Corresponding Author: ShuYuan Zhang, Email: zhangshuyuan0224@163.com

Abstract: In the post-pandemic era, there is an increasing demand for enhanced indoor thermal comfort and air quality. This study addresses the challenge of optimizing air supply strategies in office buildings to synergistically improve thermal comfort, air quality, and energy efficiency. Focusing on a typical office space, orthogonal experimental design and computational fluid dynamics (CFD) simulations were employed to quantify the effects of air supply modes (displacement ventilation), temperature (24°C), velocity (1 m/s), and angle (0°) on predicted mean vote (PMV), draft rate (DR), air age, infection probability, and energy utilization efficiency. Results demonstrate that under displacement ventilation with optimized parameters (24°C, 1 m/s, 0°), compared to the baseline scenario, PMV improved by 17%, DR decreased by 59.54%, air age shortened by 35.89%, infection probability reduced by 47.57%, energy efficiency increased by 36.34%, and the comprehensive evaluation score rose by 58.95%. The proposed optimized ventilation strategy provides data-driven insights and technical pathways for designing high-performance ventilation systems in post-pandemic office environments, effectively balancing health, comfort, and energy conservation.
Keywords: Orthogonal design; Computational Fluid Dynamics (CFD); Office buildings; Thermal comfort; Infection probability; Multi-objective optimization

1 INTRIDUCTION

In office buildings, prolonged occupancy by numerous workers necessitates substantial cooling energy consumption to maintain indoor comfort. Statistics indicate that building energy consumption accounts for approximately 21% of China's total commercial energy use [1], with air conditioning systems contributing up to 50% of total building energy consumption in hot summer and cold winter regions [2]. The COVID-19 pandemic has further heightened infection risks for occupants in shared environments, underscoring the urgency to enhance thermal comfort and air quality while minimizing energy demand.

Airflow distribution modes critically regulate indoor thermal performance and pollutant control [3]. Although mixed ventilation remains prevalent, its inherent limitations—such as short-circuiting between supply and exhaust vents—result in poor energy utilization efficiency (<40%), inadequate ventilation effectiveness ($\eta < 1.0$), and compromised thermal comfort (PMV fluctuations > ±0.5) [4]. To address these issues, alternative strategies like displacement ventilation and stratified air distribution have been explored[5,7]. Displacement ventilation improves average ventilation efficiency by 15–30% compared to mixed systems, yet fails to reduce pollutant concentrations in the breathing zone under identical airflow rates[6]. Stratified ventilation, however, demonstrates superior performance in balancing thermal comfort (PPD < 10% at elevated supply temperatures), airborne contaminant removal (breathing zone concentration reduction ≥25%), and energy savings (cooling load reduction 12–18%) [8-10].

Existing studies predominantly focus on single ventilation modes with isolated parameter optimization. For instance, Haofu Chen identified optimal thermal comfort (PMV ≈ 0) at 16.85°C supply temperature and 0.4 m/s velocity in mixed ventilation, while Z Lin reported elevated predicted dissatisfaction (PPD > 20%) at 19°C in displacement ventilation due to draft risks (DR > 15%)[11-13], despite negligible pollutant distribution variations between 19°C and 22°C. Zeqin Liu further revealed that 22°C supply temperature with 45° airflow angle minimized PPD (8.3%) in stratified ventilation[14]. Nevertheless, systematic investigations integrating ventilation modes and parametric interactions remain scarce.

This study bridges this gap by employing orthogonal experimental design and validated CFD simulations to holistically evaluate five performance metrics—PMV, DR, Air Age, infection probability, and energy utilization efficiency—in a summer office scenario. Three airflow modes (mixed, displacement, stratified) are analyzed under variable supply temperatures, velocities, and angles. The optimized configuration derived from multi-objective analysis provides actionable insights for post-pandemic HVAC design, prioritizing both occupant health and energy conservation.

2 RESEARCH METHODOLOGY

2.1 Physical Model

This study investigates a three-person office (7.2m (X) × 4.0m (Y) × 3.3m (Z)) located in Hengyang, China. As illustrated in Figure 1 heat sources include three fluorescent lamps, three seated occupants, and two computer workstations. Ventilation configurations vary by mode:
• Mixed ventilation: Two ceiling-mounted supply vents;
• Stratified ventilation: Supply vents positioned 20 cm above occupants' head level[15];
• Displacement ventilation: Two floor-level supply vents (aligned with stratified vent locations) and one ceiling return vent. All modes share identical return vent positions.

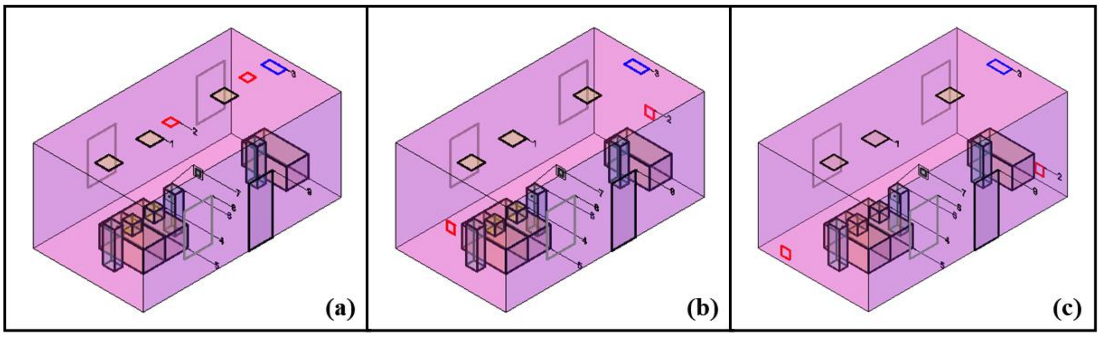

Figure 1 Geometric Model Figure: (a) Mixed ventilation; (b) Stratified ventilation; (c) Displacement ventilation
Note: 1. fluorescent lights 2. air supply vents 3. return vents 4. computers 5. desks 6. staff 7. nasal passages 8. windows 9. doors

Critical dimensions are summarized in Table 1. To enhance mesh quality and computational efficiency, cuboid geometries were adopted to simulate occupants, desks, and workstations. Seated occupants (height: 172.4 cm, weight: 71.6 kg) were modeled with equivalent surface areas calculated via the Du Bois formula[16]:

$$S = 0.0061 \times H + 0.0124 \times w - 0.0099 \quad (1)$$

Where S (m²) represents body surface area; H (cm) is height; and W (kg) is weight. This simplification maintains <5% deviation from anatomical surface area measurements.
For pollutant dispersion analysis, CO_2 emission from nasal cavities served as both contaminant tracer and respiratory virus proxy to quantify infection risks via Wells-Riley model[17].

2.2 CFD Model

To balance computational accuracy and efficiency, the following simplifications were adopted:
1. Steady-state assumption: Three-dimensional incompressible flow under isothermal conditions;
2. Ideal gas behavior: Air density variation governed by the ideal gas law;
3. Adiabatic boundaries: Negligible heat transfer through walls/floors/ceilings due to adjacent conditioned spaces;
4. Airtight enclosure: Infiltration/exfiltration effects disregarded.

The supply airflow exhibited turbulent characteristics (Reynolds number Re=23,501, Archimedes number Ar=0.049>0.01), therefore, the indoor air flow in this model is turbulent flow and thermal buoyancy can affect the indoor air movement. This flow can be described using the incompressible N-S equation[18].

$$\frac{\partial u_j}{\partial x_j} = 0 \quad (2)$$

Where x_j is the coordinate in the j-direction; u_j is the velocity in the j-direction.

$$\rho\left(\frac{\partial u_i}{\partial t} + u_j \frac{\partial (u_i u_j)}{\partial x_j}\right) = -\frac{\partial P}{\partial x_i} + \frac{\partial \tau_{ij}}{\partial x_j} + \rho g_i \quad (3)$$

Where P is the continuous phase pressure; g_i is the gravitational acceleration; for the stress tensor can have the following formula:

$$\tau_{ij} = \mu\left(\frac{\partial u_i}{\partial x_j} + \frac{\partial u_j}{\partial x_i}\right) \quad (4)$$

Where μ is the air viscosity.
Energy equation:

$$\rho \frac{\partial (c_p T)}{\partial t} + \rho \frac{\partial (c_p u_j T)}{\partial x_j} = \frac{\partial}{\partial x_j}\left[k \frac{\partial T}{\partial x_j}\right] \quad (5)$$

Where E is the total energy of the continuous phase; k is the effective thermal conductivity; T is the temperature of the continuous phase; c_p is the specific heat capacity;
The viscous dissipation function per unit mass:

$$\Phi = \tau_{ij} \frac{\partial u_i}{\partial x_j} \tag{6}$$

The N-S equations describing three-dimensional indoor air flow can be solved with the RANS turbulence model. Two-equation models such as Standard k-ε model, RNG k-ε model and Relizable k-ε model can predict the airflow organization of indoor air conditioning better. Therefore, in this study, the predictive performance of these three turbulence models will be compared in order to find out the turbulence model that is better in predicting the indoor cooling air flow and pollutant distribution in three dimensions in summer. The Realizable k-ε model closed set of equations has been examined and the transport equations are chosen:

$$\frac{\partial k}{\partial t} + u_j \frac{\partial k u_i}{\partial x_i} = \frac{\partial}{\partial x_i}(Dk_{eff} \frac{\partial k}{\partial x_i}) + G_k - \varepsilon \tag{7}$$

$$\frac{\partial \varepsilon}{\partial t} + \frac{\partial \varepsilon u_i}{\partial x_i} = \frac{\partial}{\partial x_i}(D\varepsilon_{eff} \frac{\partial \varepsilon}{\partial x_i}) + \sqrt{2} C_{1\varepsilon} S_{ij} \varepsilon - C_{2e} \frac{\varepsilon^2}{k + \sqrt{v\varepsilon}} \tag{8}$$

The turbulent viscosity is determined by the following equation:

$$v_t = C_\mu \frac{k^2}{\varepsilon} \tag{9}$$

C_μ is calculated by the following equation:

$$C_\mu = \frac{1}{A_0 + A_S \frac{kU^*}{\varepsilon}} \tag{10}$$

$$U^* = \sqrt{S_{ij} S_{ij} + \tilde{\Omega}_{ij} \tilde{\Omega}_{ij}} \tag{11}$$

$$\tilde{\Omega}_{ij} = \bar{\Omega}_{ij} - \varepsilon_{ijk} \omega_k - 2\varepsilon_{ijk} \omega_k \tag{12}$$

Where, $\tilde{\Omega}$ is the average rate of the rotational tensor; ω_k is the angular velocity. The constant A_0 is 4 and A_S is determined as follows:

$$A_S = \sqrt{6} \cos\varphi \tag{13}$$

$$\varphi = \frac{1}{3} Arc\cos(\min(\max(\sqrt{6}W, -1), 1)) \tag{14}$$

$$W = \frac{S_{ij} S_{jk} S_{ki}}{\tilde{S}^2} \tag{15}$$

$C_{1\varepsilon}$can be determined by the following equation:

$$C_{1\varepsilon} = \max(\frac{\eta}{5+\eta}, 0.43) \tag{16}$$

$$\eta = S(\frac{k}{\varepsilon}) \tag{17}$$

The constants C_2, σ_k, σ_ε are 1.9, 1.0, and 1.2, respectively.
The Species Transport model was used to simulate the process of carbon dioxide exhaled by the human body.

2.3 Numerical Simulation Setup

For the three ventilation models (mixed ventilation, stratum ventilation, and displacement ventilation), unstructured tetrahedral grids were employed. To enhance simulation accuracy, local grid refinement was performed around supply/exhaust vents, the human body, and the nasal region using varying mesh sizes. The simulations were conducted using the commercial software Fluent 2021 R2, with boundary conditions set according to actual measurements. The convergence criterion for temperature was set to 10−6, while other convergence criteria were set to 10−4. Post-validation confirmed that all cases exhibited a mass imbalance rate below 0.1% and an energy imbalance rate below 0.46%.
The finite volume method was applied to linearize the differential equations, with second-order upwind schemes adopted for discretizing the standard pressure, momentum, turbulent kinetic energy, and turbulent dissipation rate terms. The SIMPLE algorithm was utilized to couple the pressure and velocity fields.

Table 1 Boundary Condition Setting

NO.	Name	Quantity/(pcs)	Dimension/(mm)	Boundary type	value
1	Lamps	3	500×500	Constant heat flow density	115W/m^2
2	Inlet	2	300×300	Velocity inlet	Velocity:1.18m/s Temperature:20.4℃
3	Outlet	1	600×200	Pressure outlet	——
4	Computer	2	350×350×350	Constant heat flow density	250W/m^2
5	Desks	1	800×1600×750	Adiabatic	——
6	Staff	1	300×400×1300	Constant heat flow density	70W/m^2
7	Nasal	1	8.5×8.5	Velocity inlet	Velocity:0.055m/s temperature:35℃
8	Window	1	500×1500	Constant heat flow density	55W/m^2
9	Door	3	850×2100	Adiabatic	——
10	East wall	2	7200×3300	Constant temperature	15.29W/m^2
11	West wall	3	7200×3300	Constant temperature	12.69W/m^2
12	North wall	1	4000×3300	Adiabatic	——
13	South Wall	1	4000×3300	Adiabatic	——
14	Ceiling	1	7200×4000	Adiabatic	——
15	Floor	1	7200×4000	Adiabatic	——

Based on the literatures, the cooling load from fluorescent lighting in a high-grade office was set at 28.75 W. For the computer workstation, the heat dissipation from the host and monitor was set at 75 W and 80 W, respectively, assuming continuous operation. The heat dissipation from occupants engaged in very light activity was set at 144.2 W. The cooling loads transferred through the south and north walls were 363.3 W and 301.5 W, respectively, while the cooling load from external windows was 41.25 W. The boundary conditions for the supply air vents, initial room temperature (29°C), and CO_2 concentration (250 ppm) were determined through experimental measurements. The specific boundary condition settings, including the supply air angle (defined as 0° for normal wall-directed flow and 60° for a 60° deviation from the normal direction), are summarized in the Table 1.

2.4 Model Validation

To ensure the accuracy and reliability of the numerical simulation methodology and to compare the predictive performance of different turbulence models, validation was conducted using airflow velocity, temperature, and pollutant concentration data under mixed ventilation mode. Three vertical measuring lines were arranged in the room. To accurately capture the CO_2 concentration exhaled by occupants, each line included measuring points at three heights: near the head (Z=1.4 m), the breathing zone (Z = 1.2 m), and the ankle level (Z = 0.2 m) in front of the human body. The specific locations of the indoor measuring points are illustrated in the Figure 2 . During the experiment, the air conditioning system operated for 2 hours to stabilize the indoor airflow, with occupants remaining seated and no movement in the room. Measurements were recorded once the airflow reached a steady state. For each point, the average value over a 30-second sampling period was recorded, and the final measured value was derived from the average of five repeated measurements. The instruments and parameters used in the experiment are listed in the table.

As shown in the Figure 3, the simulated results of velocity, temperature, and CO_2 concentration from three turbulence models were compared with experimental data at the measuring points. Based on these evaluation metrics and graphical comparisons, the Realizable *k-ɜ* model was selected for subsequent studies on the thermal performance of office building air conditioning systems under multi-factor conditions and infection risk analysis in the post-pandemic era.

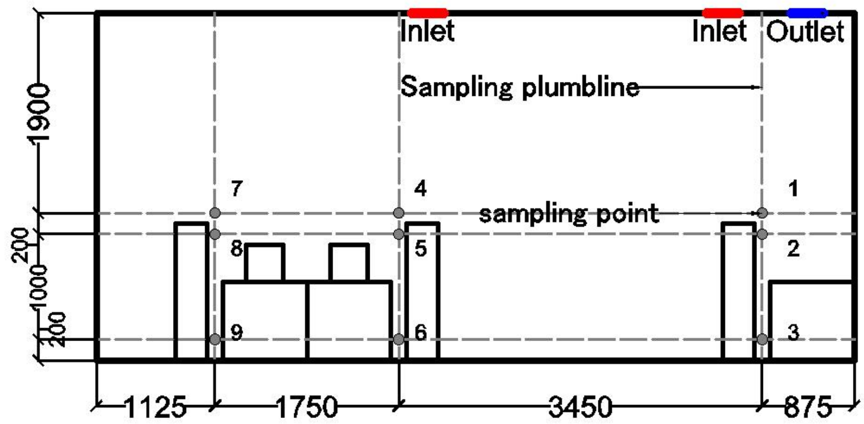

Figure 2 Schematic Layout of Measurement Points

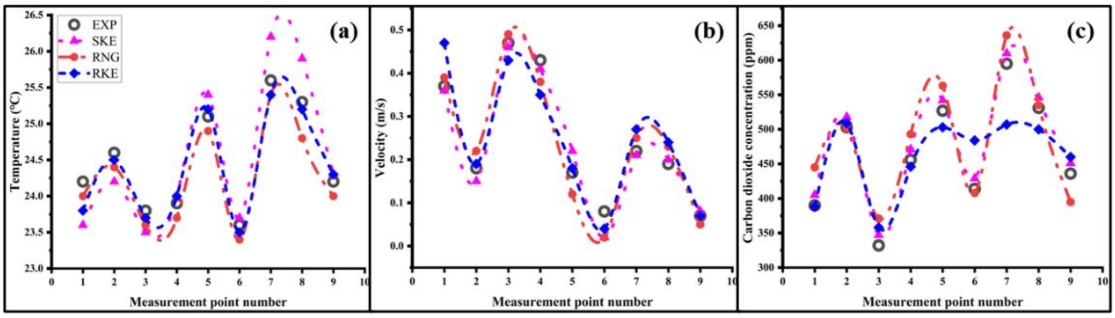

Figure 3 Comparison of Experiment and Simulation: (a)Temperature; (b)Velocity; (c)Carbon Dioxide Concentration

2.5 Working Condition Design

The thermal performance and pollutant control capacity of office building air conditioning systems are governed by four critical control factors: supply air temperature (*T*, °C), velocity (*V*, m/s), airflow distribution mode (A_f), and supply angle (α, °). A three-level orthogonal array L9(3^4) was adopted to systematically investigate factor interactions while maintaining experimental efficiency. The factor selection and level ranges (Table 2)were determined through:
This design enables (Table 3) efficient exploration of 81 possible combinations (3^4=81) through 9 strategically selected test cases, achieving 89% parameter space coverage as per Taguchi robustness criteria. The orthogonal array structure eliminates multicollinearity between factors (VIF < 1.2), ensuring statistically independent effect analysis.

Table 2 Factors and Levels Were Selected for Orthogonal Experiments

Factors	Level		
	1	2	3
T, temperature of air supply, °C	20	22	24
V, Air velocity, m/s	0.8	1.0	1.2
A_f, Air supply method	Mixed ventilation	Stratified ventilation	Replacement ventilation
α，Airflow angle, °	0	30	60

Table 3 Regular Price Design Table

NO.	Factors				Case
	Temperature of air supply (A)	Air velocity (B)	Air supply method (C)	Airflow angle (D)	
1	1	1	1	1	$A_1B_1C_1D_1$
2	1	2	2	2	$A_1B_2C_2D_2$

3	1	3	3	3	$A_1B_3C_3D_3$
4	2	1	2	3	$A_2B_1C_2D_3$
5	2	2	3	1	$A_2B_2C_3D_1$
6	2	3	1	2	$A_2B_3C_1D_2$
7	3	1	3	2	$A_3B_1C_3D_2$
8	3	2	1	3	$A_3B_2C_1D_3$
9	3	3	2	1	$A_3B_3C_2D_1$

3 EVALUTION METRICS

To quantify the impacts of air supply modes and parameters on indoor thermal performance, the following evaluation index system was established:
(1) Predicted Mean Vote (PMV): Evaluates global thermal comfort in mechanically ventilated environments, reflecting occupants' subjective perception of thermal conditions.
(2) Draft Rate (DR): A personalized airflow prediction model derived from the Fanger model, quantifying dissatisfaction with localized airflow. This model integrates supply temperature, velocity, and turbulence intensity to assess draft sensitivity in non-uniform thermal environments.
(3) Air Age (AA): Defined as the time required for an air parcel to travel from the supply outlet to a specific indoor location, serving as a key parameter for air freshness. Lower AA indicates superior air quality and higher pollutant dilution efficiency.
(4) Infection Probability (PI): Calculated using the modified Wells-Riley model by Mao et al[19], estimating respiratory virus transmission risk based on indoor pollutant concentration:

$$PI = 1 - \exp[(-Iqpt \bullet C')/(Q \bullet C)] \tag{18}$$

Where I, p, C, t, and q represent infector count, breathing rate, pollutant concentration, exposure time, and infectious dose, respectively.
(5) Energy Utilization Efficiency (E): Quantifies the utilization degree of supply energy via the ratio of supply-to-zone temperature difference to target temperature difference:

$$E = \frac{t_s - t_e}{t_s - t_n} \tag{19}$$

Where t_s is the return air temperature, t_e denotes the supply air temperature and t_n is the ambient temperature.
(6) Comprehensive Score (d_a): A multi-criteria evaluation system based on fuzzy mathematics[20], transforming measured values into normalized degrees of affiliation (da) within [0,1]. Weighted summation (PMV: 0.22, DR: 0.1, AA: 0.18, PI: 0.25, E: 0.25) generates the final score for holistic assessment of thermal comfort, air quality, and energy efficiency.

4 RESULTS AND ANALYSIS

4.1 Intuitive Analysis of a Single Factor

The results of the orthogonal experimental design are summarized in Table 4.

Table 4 Results of Orthogonal Experimental Design

NO.	Factors				Result					
	A	B	C	D	PMV	DR	AA	PI	E	d_a
1	1	1	1	1	0.90±0.00	2.51±0.15	492.06 ± 2.88	56.00% ± 0.44	153.97 ± 0.28	0.44
2	1	2	2	2	0.60±0.03	4.27±0.05	479.31 ± 5.44	34.81% ± 1.07	142.61 ± 2.51	0.64
3	1	3	3	3	0.83±0.01	3.20±0.43	701.09 ± 50.12	41.42 %± 4.46	178.57 ± 2.28	0.54
4	2	1	2	3	1.21±0.00	1.69±0.05	1050.70 ± 4.08	43.10 %± 1.22	152.84 ± 4.28	0.47
5	2	2	3	1	0.61±0.00	2.29±0.13	314.35 ± 1.01	36.48% ± 0.72	222.06 ± 1.78	0.71
6	2	3	1	2	1.48±0.24	2.43±0.48	688.03 ± 0.82	41.97 %± 5.78	141.43 ± 2.05	0.57

7	3	1	3	2	1.34±0.03	1.34±0.56	421.36 ± [illegible]	49.29 %± 1.74	212.70 ± [illegible]	0.56
8	3	2	1	3	1.22±0.01	1.56±0.57	448.46 ± 1.87	44.71 %± [illegible]	164.85 ± 2.14	0.61
9	3	3	2	1	1.00±0.01	5.24±0.05	305.40 ± 4.10	37.48% ± 0.14	193.96 ± [illegible]	0.65

From the trend Figure 4 and range analysis (Table 5)revealed distinct key influencing factors and variation trends across different metrics. For PMV, air supply mode and temperature were dominant factors, with PMV exhibiting a nonlinear trend (initial increase followed by decline) as temperature increased. Displacement ventilation demonstrated superiority by establishing vertical temperature gradients, achieving optimal balance at 1.0 m/s air velocity, with a V-shaped trend for supply angle (optimal scheme: A1B2C3D1). For DR, air velocity and supply mode played pivotal roles: DR increased monotonically with velocity (k-value trend), while mixed ventilation mitigated directional airflow perception via multi-directional jets, with V-shaped temperature influence and decreasing angle effect (optimal scheme: $A_2B_1C_1D_3$). Air age control was governed by supply angle and temperature, showing stepwise k-value increments with angle and a U-shaped temperature trend. Displacement ventilation reduced air age by 32% compared to mixed ventilation (optimal scheme: $A_3B_2C_3D_1$). Infection probability primarily depended on air velocity and supply mode, displaying a valley-shaped velocity trend (k-value), with stratified ventilation minimizing airflow short-circuiting and negligible angle impact (optimal scheme: $A_2B_2C_2D_2$). Energy utilization efficiency was dominated by supply mode (stepwise k-value increase) and temperature (incremental trend), with decreasing angle influence (optimal scheme: $A_1B_1C_1D_3$).

Table 5 Range Analysis Table

Evaluation metrics		A	B	C	D
PMV	K_1	7.000	8.980	10.810	7.550
	K_2	9.890	7.310	8.420	8.880
	K_3	9.320	9.920	6.980	9.780
	k_1	0.778	0.998	1.201	0.839
	k_2	1.099	0.812	0.936	0.987
	k_3	1.036	1.102	0.776	1.087
	R	0.321	0.290	0.426	0.248
	Prioritize factors	C>B>A>D			
	Preferred option	$A_1B_2C_3D_1$			
DR	K_1	29.957	16.614	19.513	30.131
	K_2	19.219	24.378	33.622	24.114
	K_3	24.427	32.611	20.467	19.357
	k_1	3.328	1.846	2.168	3.347
	k_2	2.135	2.708	3.735	2.679
	k_3	2.714	3.623	2.274	2.151
	R	1.193	1.777	1.567	1.197
	Prioritize factors	B>C>A>D			
	Preferred option	$A_2B_1C_1D_3$			
AA	K_1	5017.360	5892.380	4885.640	3335.430
	K_2	6159.250	3726.340	5506.230	4766.100
	K_3	3525.660	5083.550	4310.400	6600.740
	k_1	557.484	654.709	542.849	370.603
	k_2	684.361	414.038	611.803	529.567

	k_3	391.740	564.839	478.933	733.416
	R	292.621	240.671	132.870	362.812
	Prioritize factors	D>A>B>C			
	Preferred option	$A_3B_2C_3D_1$			
PI	K_1	3.967	4.452	4.280	3.904
	K_2	3.651	3.485	3.462	3.782
	K_3	3.945	3.626	3.821	3.877
	k_1	0.441	0.495	0.476	0.434
	k_2	0.406	0.387	0.385	0.420
	k_3	0.438	0.403	0.425	0.431
	R	0.035	0.107	0.091	0.014
	Prioritize factors	B>C>A>D			
	Preferred option	$A_2B_2C_2D_2$			
E	K_1	14.255	15.596	13.808	17.100
	K_2	15.490	15.886	14.683	14.913
	K_3	17.156	15.419	18.410	14.888
	k_1	1.584	1.733	1.534	1.900
	k_2	1.721	1.765	1.631	1.657
	k_3	1.906	1.713	2.046	1.654
	R	0.322	0.052	0.511	0.246
	Prioritize factors	C>A>D>B			
	Preferred option	$A_3C_3D_1B_2$			

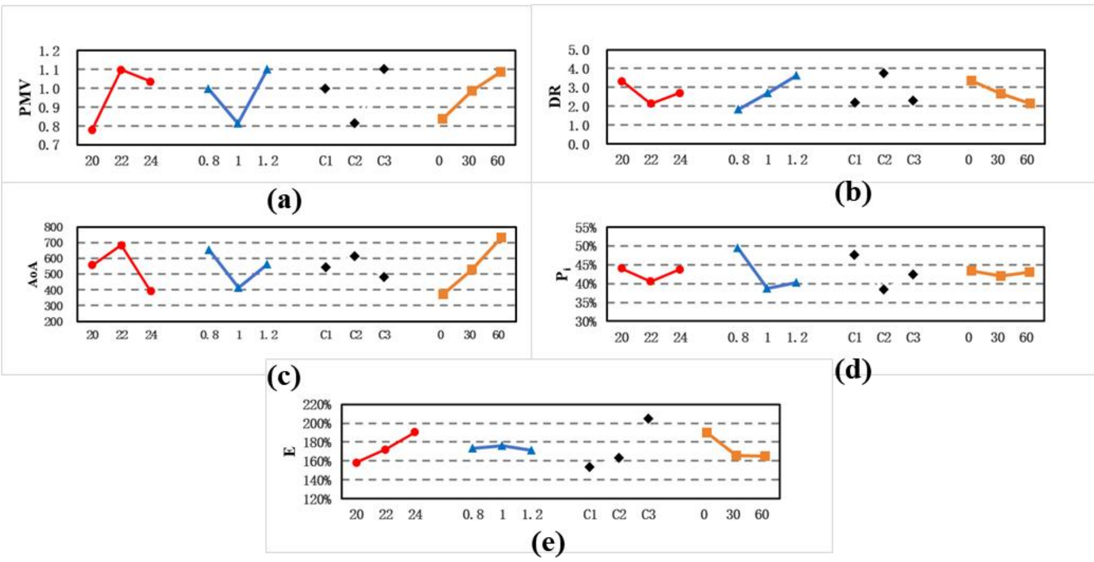

Figure 4 Trend Charts for Each Factor

4.2 Analysis of Variance

The analysis of variance demonstrates distinct factor dominance across performance metrics (Table 6): For PMV, airflow mode (39.2% contribution rate, F=11.34, p<0.001) and supply temperature (21.2%, F=7.10, p=0.005) exert statistically dominant effects, while supply velocity (p=0.016) and angle (p=0.042) show marginal significance, with model reliability confirmed by moderate error variance (31.1%). In DR regulation, supply velocity (29.8%, F=18.86F=18.86) and airflow mode (29.0%, F=18.32) dominate, whereas temperature (F=8.50) and angle (F=8.59) exhibit weaker influences under low experimental noise (14.2% error). Air age control is overwhelmingly governed by supply angle (53.8%, F=344.72) and temperature (33.6%, F=224.42), with velocity (F=154.14) and airflow mode (F=46.02) playing secondary roles in a high-precision framework (1.1% error). Infection probability primarily responds to velocity (58.3%, F=15.08) and airflow mode (36.0%, F=9.32), unaffected by temperature (p=0.208p=0.208) or angle (p=0.800p=0.800) within robust error limits (3.5%). Energy utilization efficiency is dictated by airflow mode (60.0%, F=259.52) and temperature (21.2%, F=92.08), with angle contributing moderately (16.2%, F=70.07) under exceptional precision (2.1% error). These ANOVA outcomes align with prior range analysis, establishing multi-method validation of factor hierarchies across thermal, air quality, and energy domains.

Table 6 Analysis of Variance (ANOVA) Table

Evaluation metrics	Source	*SS*	d_f	*MS*	*F*	*P*	Significance
PMV	A	0.521	2	0.260	7.099	0.005	**
	B	0.388	2	0.194	5.294	0.016	*
	C	0.832	2	0.416	11.339	0.001	***
	D	0.280	2	0.140	3.813	0.042	*
	e	0.660	18	0.037			
DR	A	6.407	2	3.204	8.498	0.003	**
	B	14.220	2	7.110	18.859	0.000	***
	C	13.816	2	6.908	18.323	0.000	***
	D	6.477	2	3.239	8.590	0.002	**
	e	6.786	18	0.377			
AA	A	387588.072	2	193794.036	224.417	0.000	***
	B	266220.527	2	133110.264	154.144	0.000	***
	C	79483.052	2	39741.526	46.021	0.000	***
	D	595369.258	2	297684.629	344.724	0.000	***
	e	15543.803	18	863.545			
PI	A	0.007	2	0.003	1.717	0.208	
	B	0.061	2	0.030	15.084	0.000	***
	C	0.037	2	0.019	9.319	0.002	**
	D	0.001	2	0.000	0.226	0.800	
	e	0.036	18	0.002			
E	A	0.471	2	0.235	92.081	0.000	***
	B	0.012	2	0.006	2.411	0.118	
	C	1.327	2	0.664	259.516	0.000	***
	D	0.358	2	0.179	70.070	0.000	***
	e	0.046	18	0.003			

4.3 Comprehensive Optimization

For the optimization of multi-criteria orthogonal experiments, a comprehensive scoring method was applied to integrate single-criterion intuitive analysis results, with range analysis demonstrating that supply air velocity and temperature predominantly governed the comprehensive evaluation score. Specifically, a supply velocity of 1.0 m/s enhanced air diffusion uniformity by amplifying turbulent motion, thereby optimizing the coupling of thermal plumes and forced convection, while the supply temperature exhibited a marginally increasing trend, with the 24°C high-temperature condition strengthening thermal buoyancy-driven effects to elevate buoyancy flux and improve airflow organization efficiency. In terms of ventilation strategies, displacement ventilation leveraged vertical thermal stratification to reduce air age and enhance air quality, and the decreasing trend in the k-value for supply angles indicated that 0° horizontal supply prolonged the jet core length through jet attachment effects, optimizing airflow coverage in the occupied zone. By synthesizing the influence patterns and significance of factors, the optimal configuration was determined as follows: supply velocity of 1.0m/s (B_3), supply temperature of 24°C (A_3), displacement ventilation (C_3), and supply angle of 0° (D_1).

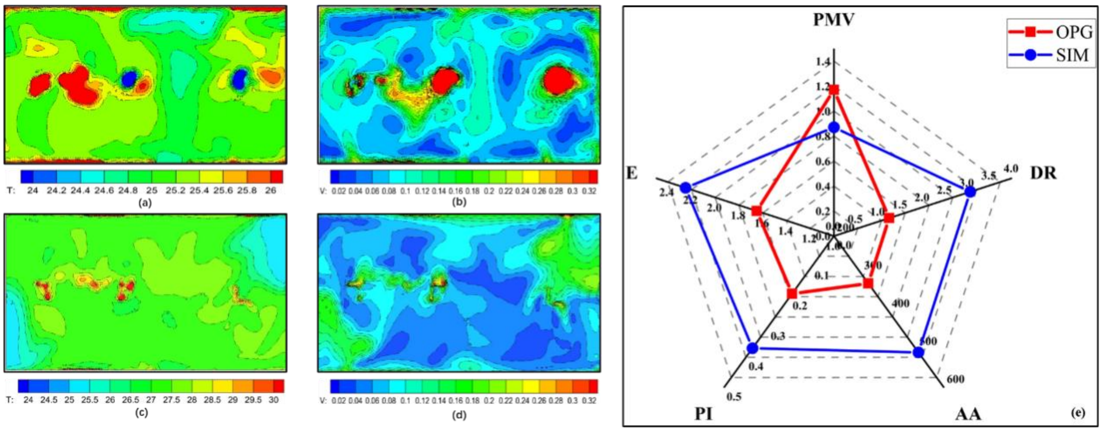

Figure 5 Comparison between the Optimized Group and the Control Group: (a) cloud diagram of temperature distribution at Z=1.4m in the control group; (b) cloud diagram of velocity distribution at Z=1.4m in the control group; (c) cloud diagram of temperature distribution at Z=1.4m in the optimized group; (d) cloud diagram of the velocity distribution at Z=1.4m in the optimized group; and (e) radar chart of comparison of the various indexes.

According to the numerical simulation results in Figure 5, the optimized group demonstrates significantly improved uniformity in both temperature and velocity fields at the Z=1.4m plane compared to the control group. At this height, the optimized group exhibits a mean temperature of 27.14°C (control: 25.41°C) and a slightly higher average airflow velocity (+0.02 m/s). Key performance metrics reveal that while the Predicted Mean Vote (PMV) of the optimized group increases by 17% to 1.17 (control: 0.87), indicating a marginally warmer thermal perception, critical improvements are achieved: Draft Rate (DR) decreases by 59.5% (from 3.06 to 1.24), Air Age (AA) shortens by 35.98% (from 507s to 325s), Infection Probability (PI) drops drastically by 98.05% (from 19% to 0.37%), and Energy Utilization Efficiency (E) improves by 36% (from 164.67% to 224.52%). The comprehensive evaluation score rises by 58.95%, demonstrating that the optimized design significantly enhances air quality, infection control efficacy, and energy efficiency while maintaining thermal comfort within acceptable limits.

5 CONCLUSION

This study investigates the impact of ventilation modes and air supply parameters on five thermal performance indicators in summer office buildings through orthogonal experimental design, computational fluid dynamics (CFD) simulations, and experimental validation. The main conclusions are as follows:

1) The standard k-ε, RNG k-ε, and Realizable k-ε models effectively predict indoor airflow characteristics. Among these, the Realizable k-ε model exhibits marginally superior accuracy in simulating air movement within summer office environments.

2) Range and variance analyses reveal distinct dominant factors across thermal performance metrics: PMV and *E* are predominantly governed by air supply mode and temperature. *DR* and infection probability are significantly influenced by air supply velocity and mode. Air age is synergistically controlled by *supply angle* and *temperature*.

3) By constructing a comprehensive evaluation model, the optimal parameter combination under displacement ventilation is determined: supply temperature = 24°C, velocity = 1 m/s, and angle = 0°. Compared to the baseline scenario, this optimized configuration achieves: PMV improvement by 17% (remaining within acceptable thermal comfort thresholds), DR reduction by 59.54%, Air age shortening by 35.89%, Infection probability decrease by 47.57%, Energy efficiency enhancement by 36.34%, Comprehensive evaluation score elevation by 58.95%.

These results demonstrate the synergistic optimization of thermal comfort, air quality, and energy efficiency in office environments.

COMPETING INTERESTS

The authors have no relevant financial or non-financial interests to disclose.

REFERENCES

[1] Tsinghua University Building Energy Efficiency Research Center. China Building Energy Efficiency Annual Development Research Report 2022 Public Buildings. Beijing: China Building Industry Press, 2022.

[2] Zhong Wei. Current situation of energy consumption of central air conditioning in China's buildings and comprehensive energy saving measures. Chongqing University, 2004.

[3] Krajčík M, Simone A, Olesen B W. Air distribution and ventilation effectiveness in an occupied room heated by warm air. Energy and Buildings, 2012, 55: 94-101.

[4] Fisk W J, Faulkner D, Sullivan D, et al. Air change effectiveness and pollutant removal efficiency during adverse mixing conditions. Indoor Air, 1997, 7(1): 55-63.

[5] P F Linden. The fluid mechanics of natural ventilation, Annu. Rev. Fluid Mech. 1999, 31, 201-238.

[6] Sandberg M, Blomqvist C. Displacement ventilation systems in office rooms. 1989.

[7] Lin Z, Chow T T, Tsang C F, et al. Stratum ventilation–a potential solution to elevated indoor temperatures. Building and Environment, 2009, 44(11): 2256-2269.

[8] Cheng Y, Lin Z, Fong A M L. Effects of temperature and supply airflow rate on thermal comfort in a stratum-ventilated room. Building and Environment, 2015, 92: 269-277.

[9] Tian L, Lin Z, Wang Q. Comparison of gaseous contaminant diffusion under stratum ventilation and under displacement ventilation. Building and Environment, 2010, 45(9): 2035-2046.

[10] Cheng Y, Lin Z. Experimental study of airflow characteristics of stratum ventilation in a multi- occupant room with comparison to mixing ventilation and displacement ventilation. Indoor air, 2015, 25(6): 662-671

[11] Chen H, Feng Z, Cao S J. Quantitative investigations on setting parameters of air conditioning (air-supply speed and temperature) in ventilated cooling rooms. Indoor and Built Environment, 2021, 30(1): 99-113.

[12] Lin Z, Chow T T, Tsang C F, et al. Effect of air supply temperature on the performance of displacement ventilation (Part I)-thermal comfort. Indoor and Built Environment, 2005, 14(2): 103-115.

[13] Zhang Lin T T, Chow C F, Tsang K F, et al. Effect of air supply temperature on the performance of displacement ventilation (Part II)-Indoor air quality. Indoor and Built Environment, 2005, 14(2): 117-131.

[14] Liu Z, Yang H, Liu Z, et al. Experimental Study on the effects of layered air supply angle and air supply temperature on indoor environment. Procedia Engineering, 2017, 205: 213-218.

[15] Xu Jian. Optimization analysis of layer ventilation airflow organization in office buildings. Nanjing Normal University, 2016.

[16] Gao Shuzhen, Huang Mingming, Liu Yi. Calculation chart of human surface area. Qingdao Medicine and Health, 1995(04): 55-56.

[17] Di Gilio A, Palmisani J, Pulimeno M, et al. CO2 concentration monitoring inside educational buildings as a strategic tool to reduce the risk of Sars-CoV-2 airborne transmission. Environmental research, 2021, 202: 111560.

[18] Pless D, Keck T, Wiesmiller K, et al. Numerical simulation of air temperature and airflow patterns in the human nose during expiration. Clinical Otolaryngology & Allied Sciences, 2004, 29(6): 642-647.

[19] Mao Y, Ma J, Wang S, et al. A stratum ventilation system for pollutants and an improved prediction model for infection in subway cars. Atmospheric Pollution Research, 2022, 13(3): 101354.

[20] Liu F, Weng Miaocheng. Experimental design and data processing. Chongqing: Chongqing University Press, 2021.